SPE 29869

Integrated Reservoir Modelling of a Major Arabian Carbonate Reservoir

J.P. Benkendorfer,* C.V. Deutsch,* P.D. LaCroix, and L.H. Landis, Exxon Production Research Company
Y. A. Al-Askar,* A.A. Al-AbdulKarim,* and J. Cole, Saudi Aramco

*SPE Members

This paper was prepared for presentation at the SPE Middle East Oil Show held in Bahrain, 11-14 March 1995.

ABSTRACT

This paper presents the results of an integrated reservoir management study of a large carbonate reservoir. Geostatistical and scale averaging tools were used to develop detailed geologic models and a simulation window model. The geostatistical simulation techniques generated realistic models of lithology, porosity, and permeability. The public-domain GSLIB software, with some custom programs for data manipulation and interactive variogram modeling, allowed for the timely and efficient construction of a multi-million cell geological model. A two-step approach to permeability modeling was successful; it allowed the straightforward integration of core and well test data and provided improved geologic models for use in history matching in flow simulations. Because of the large number of cells in the geologic model, the porosity and permeability models were scaled up for use in the simulation model. A calibrated power-law average approach to scale-up was found to work well.

The geostatistical tools used in this study are applicable to both siliciclastic and carbonate reservoirs. The two-step approach to permeability prediction is applicable whenever a significant difference exists between core-based permeability measurements and production-scale permeability. The authors suggest that such an integrated approach to reservoir management is widely applicable and yields good results.

This paper presents an overview of the methodology and techniques used to develop the geologic and simulation models for the area being studied.

INTRODUCTION

The area of study is part of a major Arabian carbonate reservoir. Oil production is from wells developed on a one-kilometer spacing, with pressure support provided by flank water injection. In the last 20 years, significant production and injection has occurred and the area has displayed two different types of water movement. Much of the area has a fairly uniform areal movement of the flood front; however, part of the study area has been characterized by rapid and erratic water movement uncharacteristic of most of the field. The objective of this study was to use current geostatistical[1,2] and scale-averaging techniques to build geologic and simulation models that integrate all of the available data in order to improve the understanding of the reservoir and to identify possible causes of the anomalous water movement.

Over the years, an ongoing program of reservoir data collection has provided a wide variety of good quality data. To analyze and model the data, the Geostatistical Software Library (GSLIB)[3], a public-domain software package, was used. This package provides a wide range of statistical and modeling tools that enable users to integrate different types of data (core, log, well test, etc.) into a comprehensive 3-D modeling system. The lithology was modeled with a sequential indicator simulation (SIS) algorithm. The porosity was modeled, by lithology, with a

References and illustrations at end of paper

sequential Gaussian simulation (SGS) algorithm. The permeability was modeled with a two-step approach; the matrix permeability was modeled with a Markov-Bayes simulation algorithm, whereas an additional component of permeability due to "large-scale" features (vugs, fractures, etc.) was modeled with a sequential Gaussian simulation (SGS) algorithm.

Figure 1 shows a schematic of the process used to develop the models. Detailed geologic models of lithology, porosity, and permeability were created using 250-meter areal gridding. Power-law averaging was used to scale the geologic models for use in a flow simulator. Several flow simulations were made to evaluate the geologic models and develop possible explanations for the cause of the unusual water movement observed in the study area. Each step in this process is discussed in this paper.

POROSITY AND LITHOLOGY MODELING

Porosity data from log analysis were used to generate porosity models. Figure 2 shows a porosity trace from a typical well in the field. The data were separated into seventeen layers which were correlatable throughout the study area and had a characteristic quality such as high or low porosity, or highly dolomitic in nature. Log and core data were collected and screened. A cell declustering algorithm (the **declus** program in GSLIB) was used to calculate declustering weights, and the data were transformed into normal scores (the **nscore** program in GSLIB).

Limestone, dolomite, and anhydrite data were obtained from core, as well as estimates made from density/neutron logs and sonic/resistivity tools. Horizontal and vertical indicator variograms were developed for each layer. For the major lithologies, spatial analysis led us to conclude that well control from one-kilometer well spacing was dense enough to allow use of indicator simulation. Lithology models were constructed using a sequential indicator simulation algorithm (the **sisim** program in GSLIB).

For layers which contained significant dolomite, separate porosity models were built by lithology to preserve the appropriate porosity distributions. Porosity models were generated using a sequential Gaussian simulation algorithm (the **sgsim** program in GSLIB). The separate porosity models were merged based on the presence of limestone or dolomite from the lithology models.

For lithology, Figure 3 shows examples of indicator variograms (limestone/dolomite) for layer 5, a heterogeneous layer containing a significant amount of dolomite. The dashed line represents the experimental variogram data; the solid line is the variogram model. In the horizontal direction, an anisotropy was observed and modeled with a primary direction of 30 degrees east of north and a minimum direction of 120 degrees east of north. For porosity, Figures 4 and 5 show horizontal and vertical variograms for limestone and dolomite in layer 5.

Figure 6 shows an example of a simulated lithology distribution for layer 5. Figure 7 shows an example of a simulated porosity distribution for layer 5.

TWO-STEP APPROACH FOR PERMEABILITY MODELING

Field observations have shown that core data alone are inadequate to explain all of the permeability that exists in this field. Pressure buildup tests show values of permeability-thickness several times that predicted by core analysis. (Also, flowmeter surveys in the area commonly show intervals of highly-confined flow.) Furthermore, trends evident in field performance data (water arrivals, water cuts, and salinity) show flood front movement at a rate much faster than anticipated in parts of the field, indicating that permeabilities are much greater than those measured in core analysis. Consistent with these field observations, previous simulation studies of this area have shown that permeabilities must be increased several times above the core values to obtain an acceptable match of field performance history.

Several factors appear to contribute to this observed discrepancy. The factors include:

(1) Core recovery is poor in the presence of fractures or large vugs, and in an interval of very high porosity at the top of the reservoir.

(2) Core samples selected for core analysis tend to be fairly uniform to avoid problems in testing. As a result, the permeabilities measured in routine core analysis tend to be low.

(3) Fractures and fracturing associated with faults may be a major contributor to the permeability and observed field performance.

Definition of Terms

To build more effective geologic models, a methodology was developed to incorporate both the well test data and core permeability measurements into the construction of geologic models of permeability. The procedure used for this process is outlined in the two columns on the right of Figure 1. Total reservoir permeability was divided into two components which we have termed "matrix" permeability and "large-scale" permeability. Each component was modeled separately using geostatistical techniques. At the end of the process, the two components were recombined to give total permeability.

"Matrix" permeability is defined as the permeability developed from values measured in core analysis. "Large-scale"

permeability represents the additional permeability, above the values measured in core, reflecting the observed field performance. The sum of these two components represents the total permeability, and is referred to as "reservoir-scale" permeability.

For further clarification, the reservoir-scale permeability can be expressed as the sum of the matrix (core) values plus the additional permeability (large-scale) as follows:

$$k_{\substack{\text{reservoir}\\\text{scale}}} = k_{\text{matrix}} + k_{\substack{\text{large}\\\text{scale}}} \quad \ldots\ldots(1)$$

Rearranging equation 1 gives:

$$k_{\substack{\text{large}\\\text{scale}}} = k_{\substack{\text{reservoir}\\\text{scale}}} - k_{\text{matrix}} \quad \ldots\ldots(2)$$

Assuming that the "reservoir-scale" permeability is measured by pressure buildup and falloff tests, it can be replaced by a "well test" term:

$$k_{\substack{\text{large}\\\text{scale}}} = k_{\substack{\text{well}\\\text{test}}} - k_{\text{matrix}} \quad \ldots\ldots(3)$$

Advantages of Two-Component Approach

There are several advantages to modeling the permeability in two components:

(1) It acknowledges that the permeabilities measured in well tests are significantly higher than core values for this field. Improved geologic models can be developed by incorporating these data "up-front" in the building of the geological models.

(2) "Large-scale" features and trends measured in well tests can be identified and modeled separately from core data.

(3) By separating these components during the geostatistical modeling process, this approach preserves the integrity of both the core data and the extra permeability measured in field tests and seen in the field performance.

MATRIX PERMEABILITY

Core porosities and permeabilities were used to develop the matrix permeability models using Markov-Bayes simulation (the **mbsim** program in GSLIB). Core data were available for 27 wells, which represents 15% of the total wells in the study area. Because of the limited sample size (relative to log data), geologic and statistical criteria were used to group core data. Distinct crossplot groups were obtained by merging data from layers 2 to 11 to form group 1, and data from layers 12 to 17 to form group 2 (see Figure 2 for layers). Each of these major groups was also separated by limestone and dolomite making a total of four porosity/permeability crossplot groups. Matrix permeability models were built, by lithology, for each layer. The final matrix permeability models were developed by merging the separate models together using the lithology models.

Markov-Bayes Algorithm

The Markov-Bayes (**mbsim**) approach was chosen for modeling matrix permeability because it builds models with spatial continuity through the use of the variogram while still honoring the bivariate relationship between porosity and permeability (i.e., the crossplot). The traditional approach of developing a linear transform for the porosity/permeability data does not capture the variability in the bivariate relationship and results in smoothing of high and low permeability values. In addition to core measurements at well locations, **mbsim** also allows use of additional data for conditioning the models.[4] For this study, the porosity models were incorporated as additional data to build spatial continuity that is closely related to the porosity model and honors the variability of the crossplot.

Each crossplot was calibrated for input to **mbsim** using a GSLIB utility program called **mbcalib**. The general concept of the calibration procedure can be described with the aid of Figure 8, a crossplot for group 1 limestone. Bivariate statistics are printed above the plot. (A linear transform is provided for reference but is not used for modeling matrix permeability.) The crossplot has been divided into 8 porosity classes and 15 permeability classes. Permeability class frequencies (percentage) for each porosity class are printed in the corner of each porosity/permeability class. The number of porosity and permeability classes were selected to provide adequate representation of the crossplot to the extent that adding more classes does not affect the outcome of the simulation. The **mbcalib** program calculates factors to weight the porosity model relative to the variogram model for predicting permeability. Further information on the Markov-Bayes procedure is contained in References 3 and 4.

Variogram Modeling

An interactive modeling program was used to develop variogram models to match the experimental data. Experimental variograms from core permeability data revealed good vertical continuity; however, the limited sample size made it difficult to develop variogram models for horizontal continuity. Experimental horizontal variograms were analyzed for 20 different directions at 15 degree increments; however, erratic behavior was observed in all layers and variogram models could not be fit to the experimental data.

In the absence of sufficient experimental evidence of horizontal continuity, porosity variograms were scaled to build permeability variogram models that "borrow" horizontal continuity from the porosity model while preserving the vertical

continuity observed in core data. First, we matched vertical continuity observed in each layer as closely as possible by reducing the range parameters for each porosity variogram. Our analysis showed that the vertical variogram ranges were approximately one-half the ranges of porosity for equivalent samples. Therefore, this factor was used to calculate ranges for the horizontal permeability data relative to the equivalent porosity data. The resulting permeability variograms are similar to the porosity variograms but the range of continuity, both vertically and horizontally, is 50% lower. Figure 9 shows examples of the vertical and horizontal variograms used for matrix permeability in layer 5.

Two matrix permeability models were constructed for each layer using the separate limestone and dolomite porosity/permeability crossplots. The final matrix permeability model was generated by combining the limestone and dolomite models using the geostatistical model of lithology developed earlier.

LARGE-SCALE PERMEABILITY

We have defined "large-scale" permeability as all additional permeability in the reservoir which has not been measured in core data. Assuming that the well tests measure the sum of the matrix and large-scale components, the large-scale component can be calculated by subtracting the core-based matrix values from the well test permeability. To accomplish this, foot-by-foot values of well test permeability were calculated by merging well test data with open-hole flowmeters, and allocating the well test permeability-thickness according to percent flow as indicated by the flowmeter survey. The foot-by-foot values of large-scale permeability were then calculated as the difference of well test permeability minus the values of matrix permeability. (The matrix permeabilities were extracted from the geostatistical model of matrix permeability described earlier for the 250-meter cell in which the well lies.)

The flowmeter surveys were selected as the best method to distribute the well test values of permeability-thickness. For this study, we have assumed that the flowmeter surveys provide an acceptable representation of the formation away from the well, and not just near-wellbore anomalies. While flowmeter surveys have drawbacks, our view is that they still provide a good first approximation of the reservoir permeability distribution.

In general, the total reservoir-scale permeability, as estimated from well tests and flowmeters, is greater than the matrix permeability for this field. However, if the value of matrix permeability was greater than the well test/flowmeter permeability, the value of the large-scale permeability would be negative. When this occurred, the value was reset to zero for the purposes of this study. The geostatistical programs are able to handle zero values in the modeling process. When the final reservoir-scale permeability model is constructed, the zero values of large-scale permeability are filled in with matrix values.

Next, the large-scale permeabilities were analyzed and variograms developed for each layer. Geologic models of the large-scale permeability were generated using a sequential Gaussian simulation algorithm (the **sgsim** program in GSLIB).

Data Analysis and Variogram Modeling

Prior to development of variograms, the large-scale permeabilities were analyzed. Figure 10 shows a histogram and probability plot of large-scale permeabilities for layer 5 on a linear scale. Figure 11 shows the same data on a logarithmic scale.

Despite the fact that the data are displayed on a logarithmic scale, the plots show that the distribution is skewed towards low values.* A few very large values of permeability occur around 5 to 7.5 darcies. These large values occur in limited intervals in a few wells and probably represent fractures. Our current view is that these may represent a separate population of fractures which are poorly sampled. The data indicate that wells in the field only occasionally intersect such large fractures, or only some of the fractures are contributing to flow into the wellbore. These values were included in the large-scale modeling; however, the inclusion of these values does not have a significant effect on the resulting models because they represent a small fraction of the total population. While they appear to represent a population that is poorly sampled, they will probably have a significant impact on fluid flow in much of the area, and therefore should be modeled either as a separate population using geostatistical techniques (and a larger sample of data) or as a discrete phenomenon (See "Suggestions for Future Work").

The two-component approach for modeling of permeability highlights some interesting features in the data. To illustrate, Figure 12 shows a histogram and probability plot of matrix and large-scale permeabilities for layer 2. Figure 13 shows a similar plot for layer 5. Layer 2 is predominantly limestone, while layer 5 has a mix of limestone and dolomite. As a result, the distributions for layers 2 and 5 are markedly different. In layer 5, the matrix and large-scale permeability distributions appear as two distinct populations indicating the highly variable permeability in this predominately dolomite layer. The matrix (core-measured) values tend to be low, while the large-scale values reflect the existence of vugs and fractures not sampled in the core data.

*Because the display is on a logarithmic scale, the zero values (matrix greater than well test) are not displayed in the cumulative probability. For layer 5 this represents 21 percent of the total.

After analyzing the data, variograms were developed for each layer to describe the spatial distribution and continuity of the large-scale permeability. Experimental variograms were generated in fifteen degree increments to try and identify directionality in the large-scale permeabilities. If faults or bands of fractures ran in an east-west or north-south direction, then wells would fall in areas of highs and lows and directionality would be seen. However, a detailed analysis of directional variograms from each layer did not show any clearly defined directionality. While areas of more intense fracturing may exist, they may be poorly sampled because of the current relatively large spacing of wells. Because of the lack of any clearly defined directionality, isotropic variograms were used.

Figure 14 shows the horizontal and vertical variogram for large scale permeability in layer 5. The vertical variogram shows good continuity for the large-scale permeabilities. Note that the experimental data points do not increase to a sill of one, even though this is normal scores data. The most probable explanation for the occurrence of this lower than expected sill is the relatively uniform profile of the large-scale permeability. Recall that the flowmeter data were used to generate permeability profiles from well test data. However, the flowmeter data are fairly coarse and data are chosen over intervals which may be 5 or 10 feet in length. As a result, the calculation of the variogram would tend to average in a large quantity of values which are essentially the same, thus keeping the average from reaching a sill of one as normally expected in normal scores data. Since the **sgsim** program is based on normal scores, the final variogram models were scaled to a value of one.

The horizontal variogram for layer 5 is shown at the bottom of Figure 14. While there is a good fit of the variogram model in this layer, there is actually a large amount of uncertainty in the range of the large-scale variograms. We recommend that future modeling work include testing of the sensitivity of simulation model results based on different ranges of large-scale variograms. For example, the ranges of the large-scale variograms could be halved or doubled to see the effect on water movement in the simulation model.

Geostatistical Simulation of Large-Scale Permeability

The permeability realizations were generated using the sequential Gaussian simulation (**sgsim**) program in GSLIB. The input data were the individual well strings of large-scale permeability and the large-scale variograms. The program honors the primary variable as local conditioning data (values of permeability at well locations), the conditional cumulative distribution function (the univariate distribution of the permeability data), and the variograms of the permeability (spatial distribution and continuity).

SCALE-UP PROCEDURE

Having generated models of matrix and large-scale permeability, the two models were added together to obtain a geologic model of total reservoir-scale permeability as defined by Equation 1. However, this geologic model contained far too many cells (4,069,970) and was not feasible for use in reservoir simulation with current computer resources. The power-law averaging technique[4] was used to scale-up the geologic model for flow simulation in a model with 79,764 cells.

Power-law averaging can be defined by the following equation:

$$k_{power} = \left[\frac{\sum_i h_i a_i k_i^{\omega}}{\sum_i h_i a_i} \right]^{1/\omega} \quad \text{.....(4)}$$

where k_i is the i^{th} permeability value, h_i is the i^{th} thickness, and a_i is the fractional area of cell i.

The power-law parameter, ω, was calibrated by running a small, one-phase flow simulator on randomly selected areas of the geologic model. First, 300 elements of the geologic model were selected randomly. Second, effective permeabilities and corresponding ω's for the x, y and z directions were computed for each element using a single-phase flow simulator. Finally, the 300 ω values for the vertical direction and the 600 ω values for the horizontal directions (x and y) were averaged to a single value of ω for development of permeability arrays for the flow simulation. The calculated values of ω were distributed symmetrically about a mean of about 0.6 with a standard deviation of about 0.1. This distribution was considered sufficiently narrow to justify the use of the power-law averaging technique.

The average value of ω for horizontal flow was 0.6. For comparison, the classical averaging methods can be considered as special cases of power-law averaging: ω=1 corresponds to arithmetic averaging, ω=0 corresponds to geometric averaging, and ω=-1 corresponds to harmonic averaging. The average value for vertical flow was -0.6, higher than the traditional value for a harmonic average.

VERTICAL PERMEABILITY

Vertical permeability was calculated from reservoir-scale horizontal permeability prior to scale-up. Crossplots of vertical and horizontal permeability versus porosity were compared using moving-window statistics. The results showed that the distribution of vertical and horizontal permeabilities were similar for each porosity class, and that the average vertical permeability was consistently slightly less than the average

horizontal permeability. Based on these results, the following equation was used to calculate vertical permeability prior to scale-up:

$$LOG(k_v) = 0.9 * LOG(k_h) \quad \text{.....(5)}$$

where k_v is vertical permeability and k_h is horizontal permeability.

FLOW SIMULATION RESULTS

A flow simulation model was constructed and four history match runs were completed. The purpose of the runs was to evaluate the usefulness of the geostatistical techniques and the two-component approach to modeling permeability. In addition, analysis of the history matches provided an opportunity to investigate theories which may explain the unusual water movement in the area and differences observed between model and field performance.

Seventeen vertical layers were used along with a 68 by 69 areal grid giving a total of 79,764 cells. The simulation was run for 53 years with most of the production and injection occurring in the last 20 years.

Figure 15 shows the horizontal permeability for layer 5. The study area is outlined in the center of the model and represents the scaled-up array of total reservoir-scale permeabilities developed in this study. For comparison, it is surrounded by permeabilities from a previously history-matched model of the field. The new permeability array fits in well with the surrounding area from the previous model and supports the validity of the new permeability model and the two-component approach by which it was developed.

Initial Flow Simulation

A flow simulation (referred to as HM1) was run for the 53 years of history. Results are shown in Figures 16 and 17. In Figure 16, the top frame compares the average model and field pressure versus time for producers in the study area. The bottom frame shows a plot comparing the average model and field water cut.

Figure 17 shows an areal comparison of the model and field flood front. The shaded areas illustrate the calculated flood front advance with time. The solid line represents the interpreted flood front at 1985 based on first water arrivals. (The model flood front has been defined as a 0.1 percent change in model water saturation within a column of blocks. In other words, the flood front is considered to have arrived at a model location if the water saturation has increased by 0.1 percent since the beginning of history.)

In summary, the initial flow simulation showed:

(1) The calculated pressures were somewhat low, but matched the general trends of the field data.

(2) Calculated water advance was relatively uniform areally. As a result, the model compared well with the field in areas of relatively uniform water advance, such as the southeast and western parts of the model; however, in the area of rapid water advance in the middle of the study area, the model did not match field performance.

Based on the results of the initial flow simulation, we concluded that in areas of relatively uniform water advance, the geostatistical techniques provided a good initial match of areal and vertical water movement. Since this "relatively uniform" type behavior is typical of most of the field outside the study area, the techniques used in this study will be useful for building models of other areas of the field.

Additional Flow Simulation Results

In the next stage of the study, we made three additional flow simulations to explore possible explanations for the discrepancies observed between the model and field performance in the area of rapid water advance.

After a review of all the available data, we developed a working hypothesis that the failure of the initial model to match the rapid water advance was due to fracture development in this area. Several recent borehole-imaging logs indicate the presence of vertical fractures in wells in this area.

This theory was tested in three additional simulations. Fracturing was simulated by increasing permeabilities in layers which were predominately dolomite and in thin, low-porosity layers, based on the assumption that the rocks in these layers were most subject to fracturing.

Figure 18 shows a comparison of the pressure and water cut comparisons for the first and last flow simulations (HM1 and HM4). Calculated pressures and water cuts are higher in HM4 due to the increases in permeability and changes in permeability stratification which were made to increase the movement of water into the field.

Figure 19 shows an areal comparison of the model and field flood front at selected times. Compared with HM1 (Figure 17) significant improvements were made in matching the field observed flood front in the middle of the study area.

The results of the additional flow simulations provide support for the hypothesis that the geostatistical models did not adequately capture the effects of the vertical fractures. A review of the data showed that fractures were not adequately sampled in the study for two reasons. First, vertical wells do not intersect a representative number of vertical fractures and their impact on fluid flow is not adequately represented. Second, in the area of rapid water advance, the number of open-hole

flowmeters were limited. As a result, much of the well test data in this area were not used in the modeling process.

SUGGESTIONS FOR FUTURE WORK

While the geostatistical techniques were successful in modeling the areas of relatively uniform flood front movement, the lack of adequate sampling of fractures is needed for improvements in the reservoir description. Further analysis of flowmeter surveys, additional borehole-imaging logs, and horizontal wells can provide more data on the existence of vertical fractures. In addition, information from seismic surveys would provide useful information on the locations of possible faults and associated high fracture densities. With this additional data, geostatistical techniques could be used to incorporate fractures into the geologic models. Alternatively, the data may be used as guidance for modeling of faults and fractures as discrete phenomena.

We also suggest that use of multidisciplinary teams for similar studies provides an effective approach for integrating all the data "up-front" in the construction of geologic models.

Finally, the impact of different ranges for the "large-scale" permeability variograms should be investigated. There is considerable uncertainty in the ranges for permeability, and the effect of different ranges on simulation results should be tested.

CONCLUSIONS

Overall, the two-step approach for modeling permeability worked well in this project and should be applicable to situations where a significant difference exists between core-based permeability measurements and larger-scale permeability. It allows the straightforward integration of core and well test data and simplifies history matching by providing better geologic models of permeability. It can also provide a better understanding of the data because each component is analyzed independently, and separate spatial "trends" caused by depositional or post-depositional processes can be identified. Furthermore, by modeling the components separately, different spatial "trends" in the matrix and large-scale components are preserved in the final geologic models.

Geostatistics provides a scientifically based, methodical approach for developing reservoir characterizations within a consistent framework. The public-domain GSLIB software package, along with some custom programs for data manipulation and interactive variogram modeling, allowed for the timely and efficient construction of the geological models. The techniques also allowed integration of a wide range of geologic and field performance data into a comprehensive 3-D modeling system.

Initial flow simulations showed that the geostatistical techniques (as used in this study) worked best in the areas of "more uniform" water advance. Since much of the field has experienced a similar type flood front advance, these techniques can be successfully applied in the development of future geologic models.

In areas of rapid water advance, the reservoir description from the initial geostatistical models did a poor job of simulating field performance. Our view is that the most likely cause of the rapid water advance is the existence of vertical fractures (and possibly faults) and these were not adequately sampled in the data used for modeling this area. Seismic surveys, additional borehole-imaging logs, and horizontal wells can provide more data on the existence of vertical fractures, and geostatistical techniques can be used to incorporate fractures into future geologic models.

NOMENCLATURE

a	=	fractional area of cell
γ	=	variogram function
h	=	cell thickness
k	=	absolute permeability
ω	=	power-law parameter

ACKNOWLEDGMENTS

The authors thank Saudi Aramco, the Saudi Arabian Ministry of Petroleum and Mineral Resources, and Exxon Production Research Company, for permission to publish this paper.

REFERENCES

1. Haldorsen, H.H. and Damsleth, E.: "Stochastic Modeling," *JPT*, April, 1990, pp. 404-412.
2. Isaaks, E.H. and Srivastava, R.M.: *An Introduction to Applied Geostatistics*: Oxford University Press, New York, 1989.
3. Deutsch, C.V. and Journel, A.G.: *GSLIB: Geostatistical Software Library and User's Guide*, Oxford University Press, New York, NY, 1992.
4. Zhu, H., and Journel, A. G.: "Formatting and Integrating Soft Data: Stochastic Imaging via the Markov-Bayes Algorithm," *Geostatistics Troia '92*, Volume 1, pp. 1-12, Kluwer, Dordrecht, Holland, 1993.
5. Deutsch, C. V., "Calculating Effective Absolute Permeability in Sandstone/Shale Sequences," *SPE Formation Evaluation*, September, 1989.

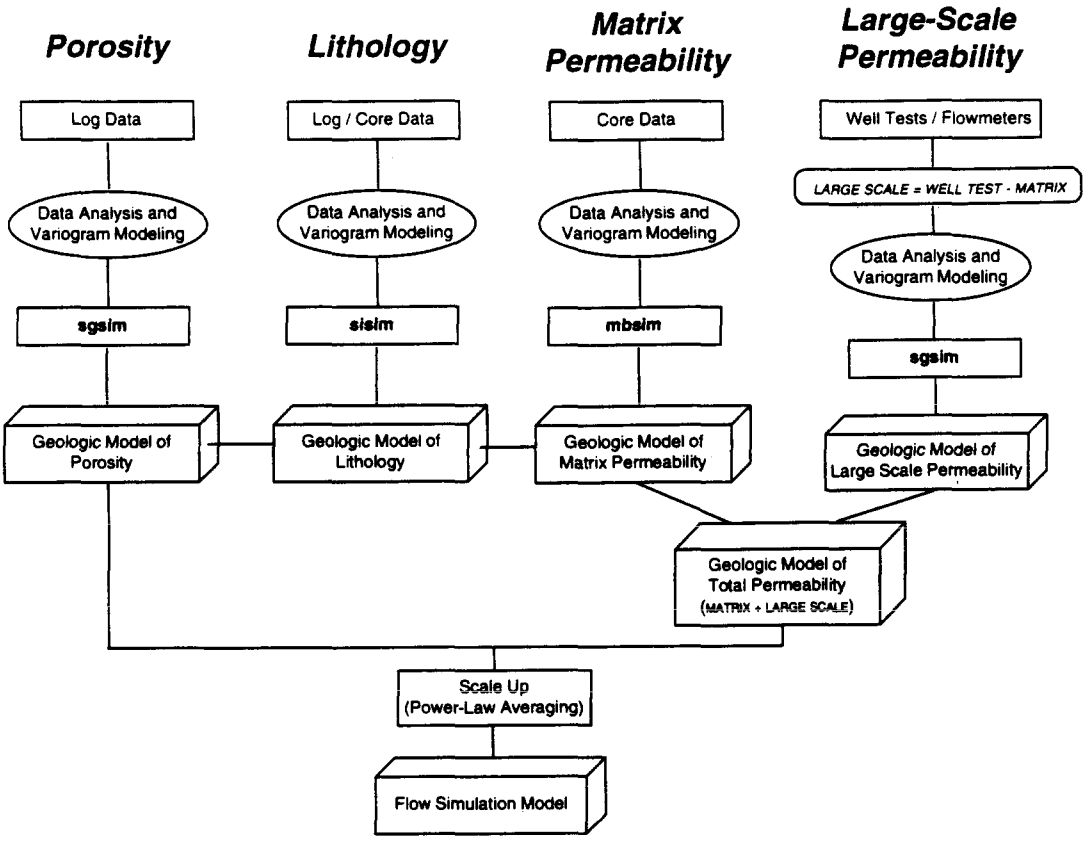

Figure 1: Schematic of Modeling Process

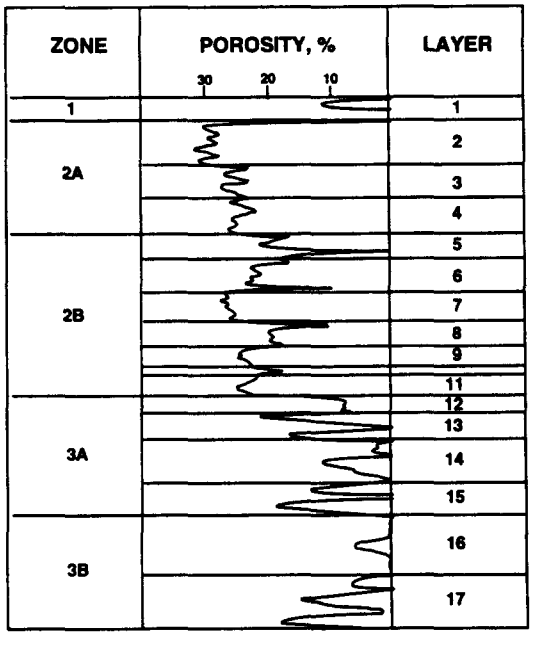

Figure 2: Model Layering

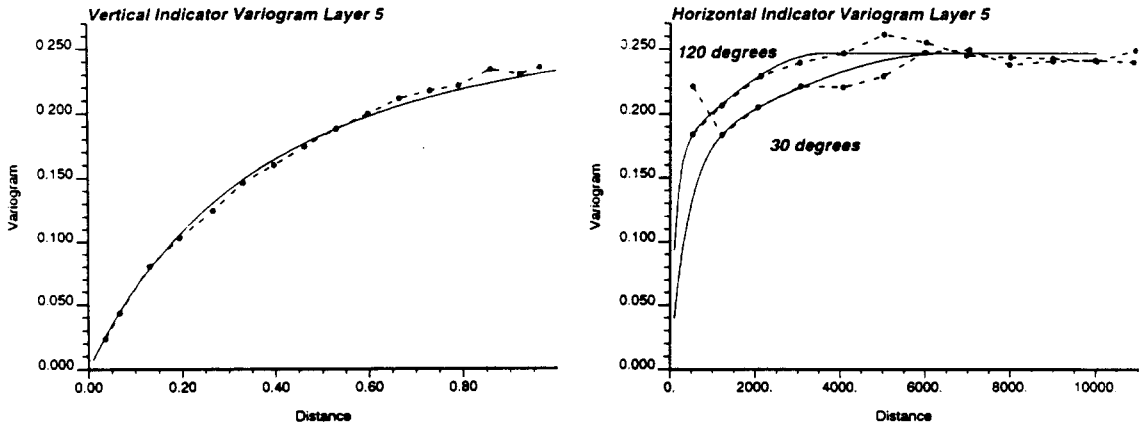

Figure 3: Vertical and horizontal lithology indicator variograms for layer 5

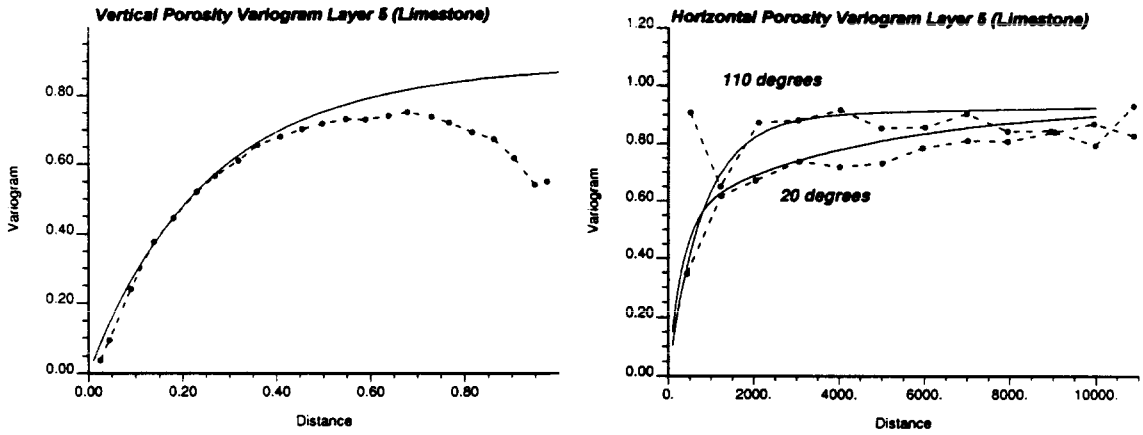

Figure 4: Vertical and horizontal porosity variograms for limestone

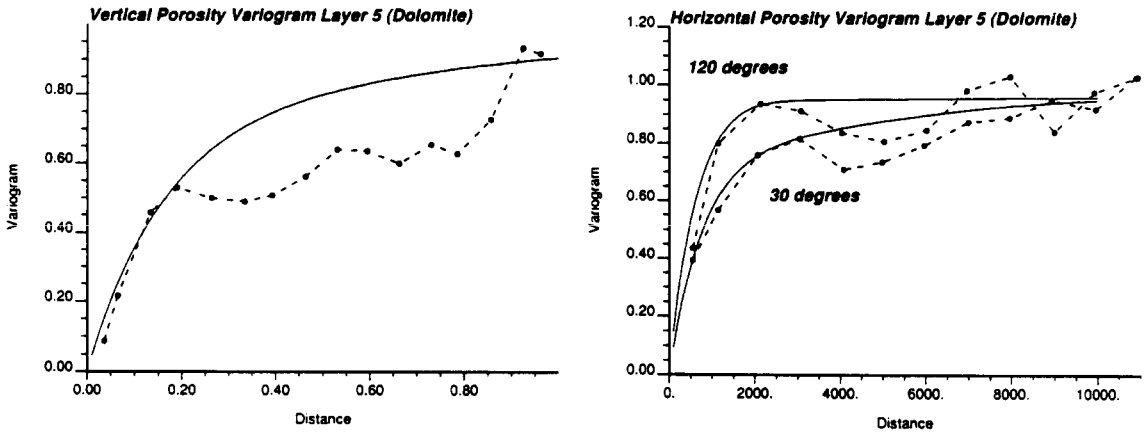

Figure 5: Vertical and horizontal porosity variograms for dolomite

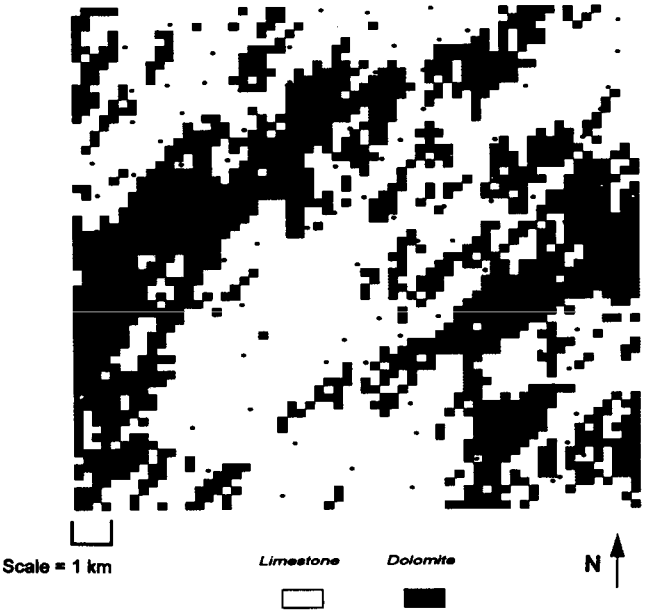

Figure 6: Example of lithology distribution

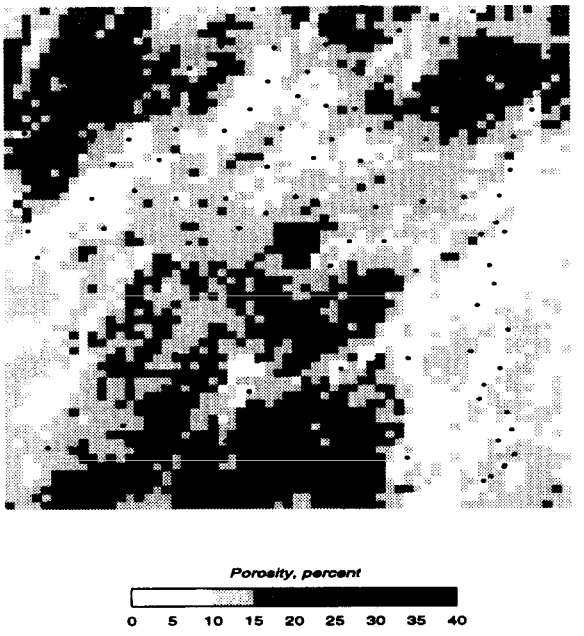

Figure 7: Example of porosity distribution

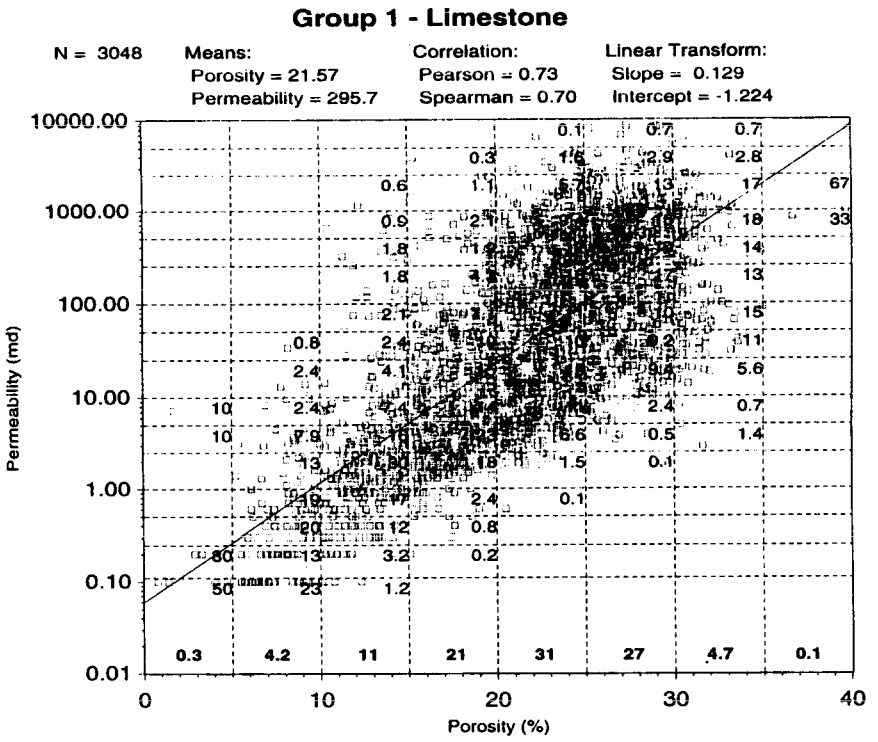

Figure 8: Crossplot for Group 1 limestone

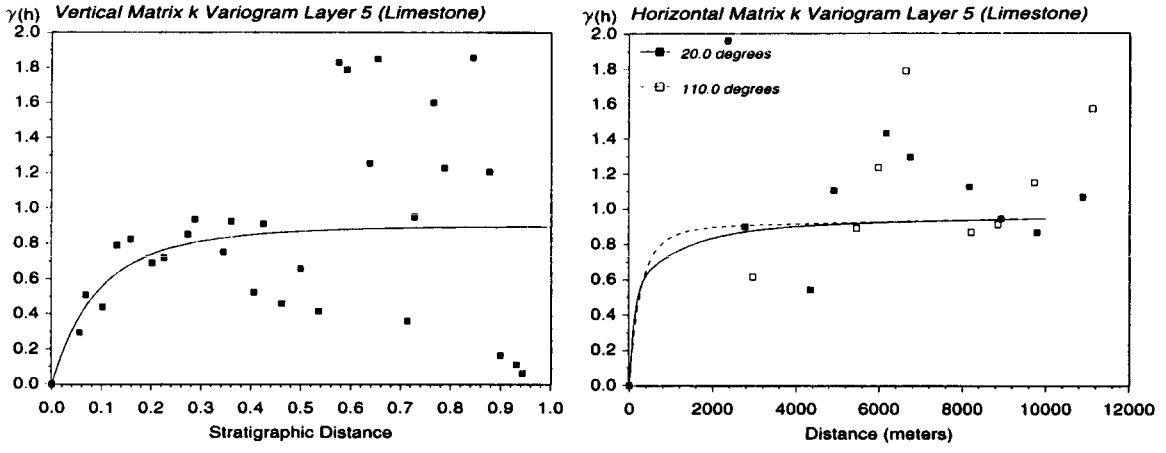

Figure 9: Vertical and horizontal matrix permeability variograms for layer 5 (limestone)

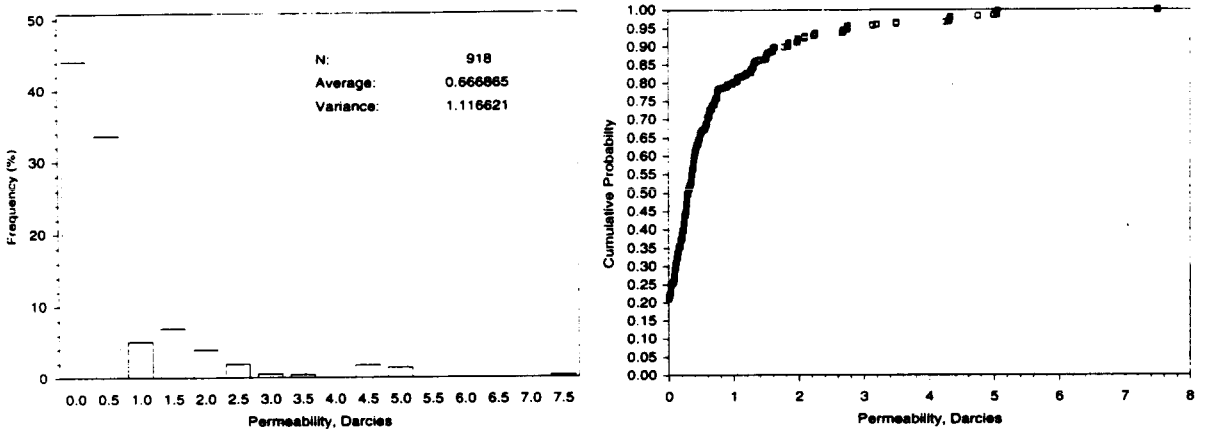

Figure 10: Histogram and probability plot for large-scale permeability (linear scale)

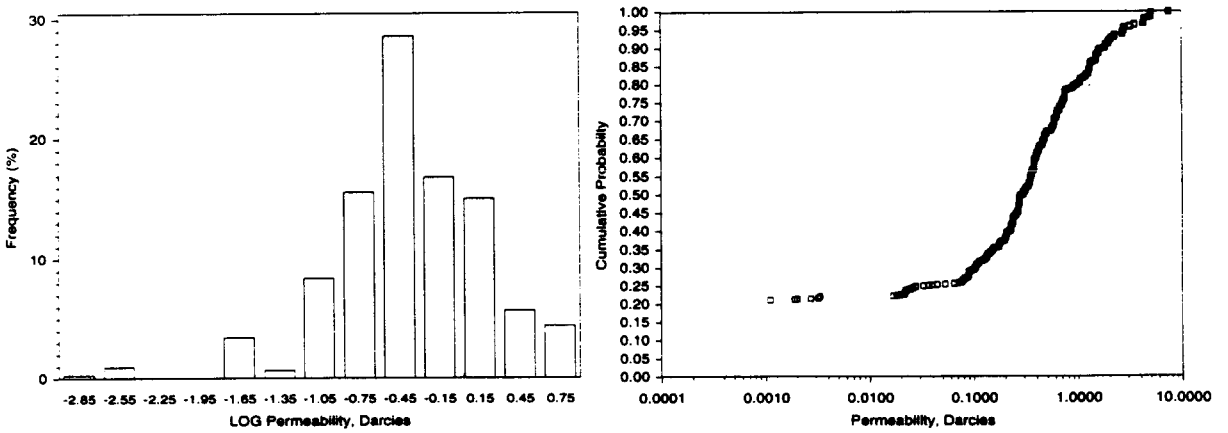

Figure 11: Histogram and probability plot for large-scale permeability (logarithmic scale)

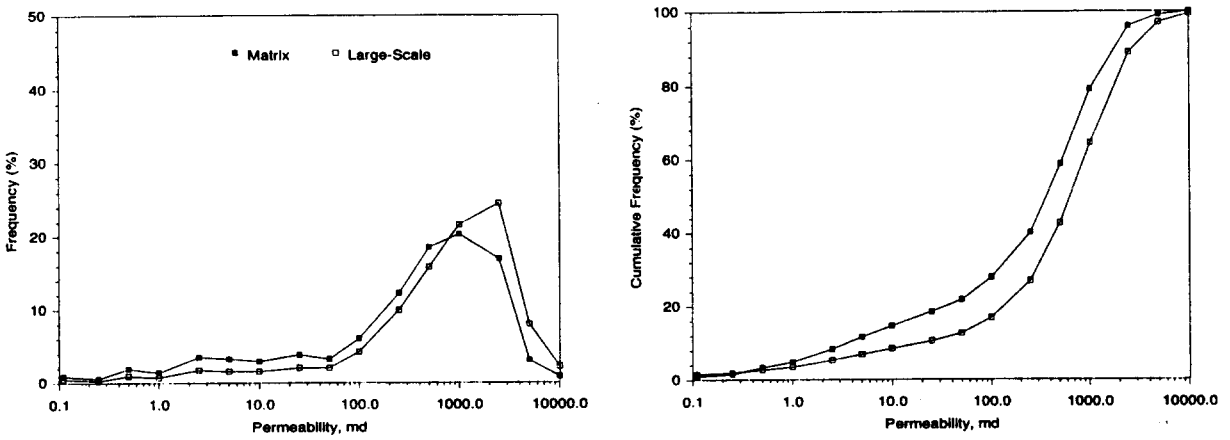

Figure 12: Histogram and probability plot for matrix and large-scale permeability - Layer 2

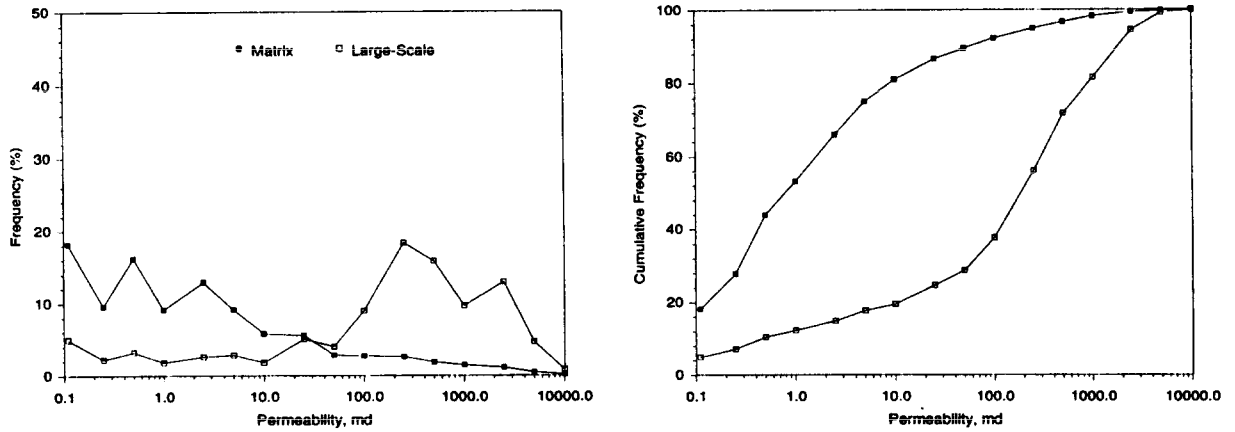

Figure 13: Histogram and probability plot for matrix and large-scale permeability - Layer 5

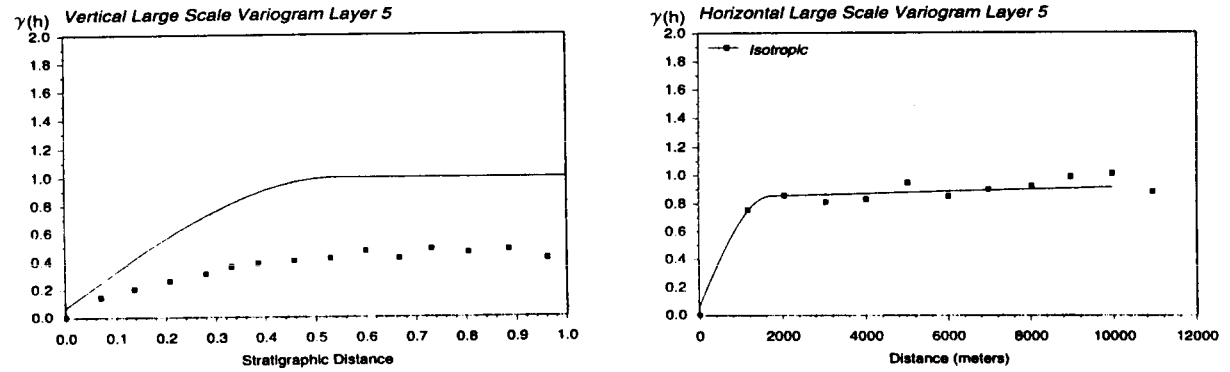

Figure 14: Vertical and horizontal large-scale permeability variograms for layer 5

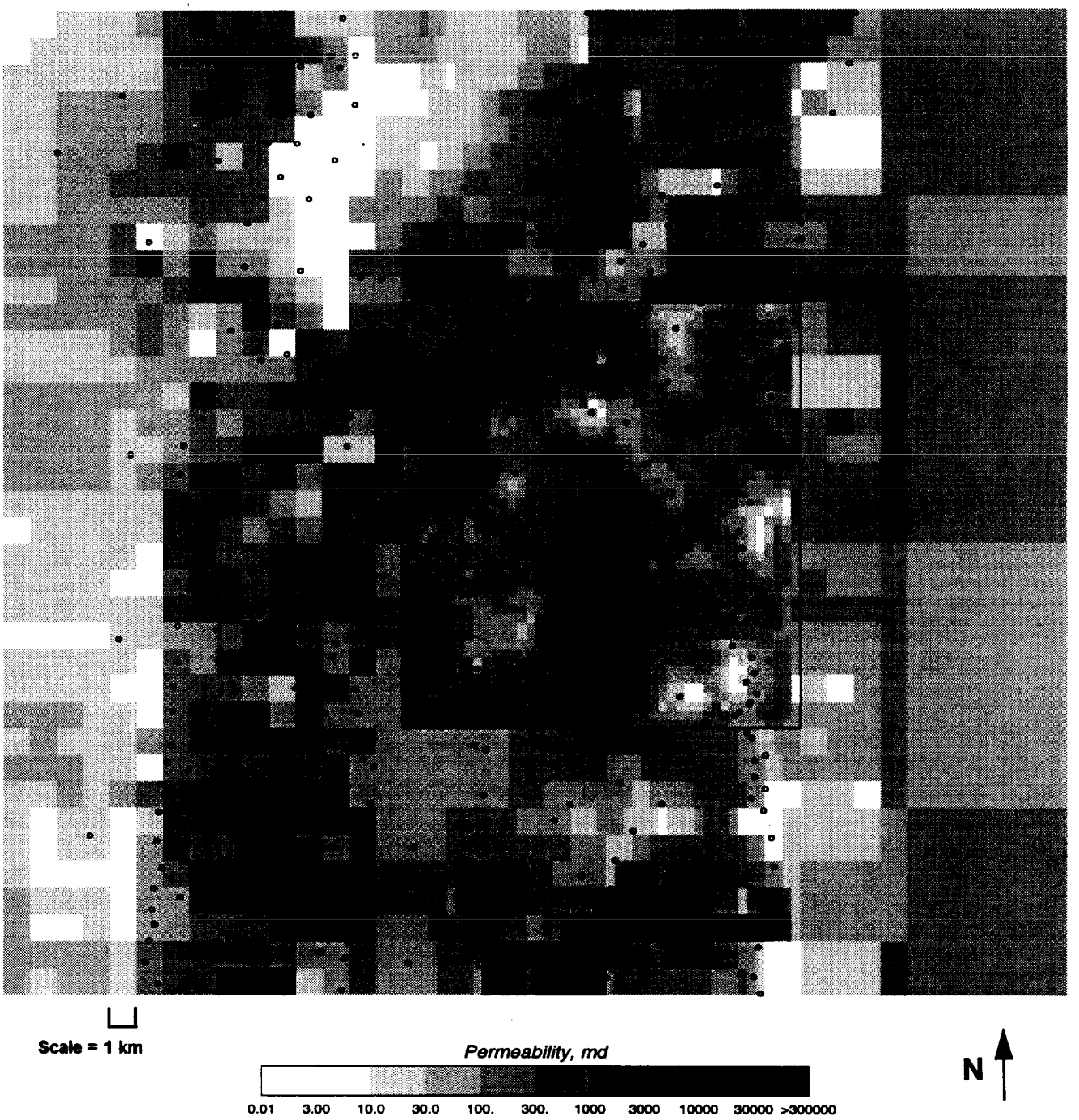

Figure 15: New permeability array embedded in matched model

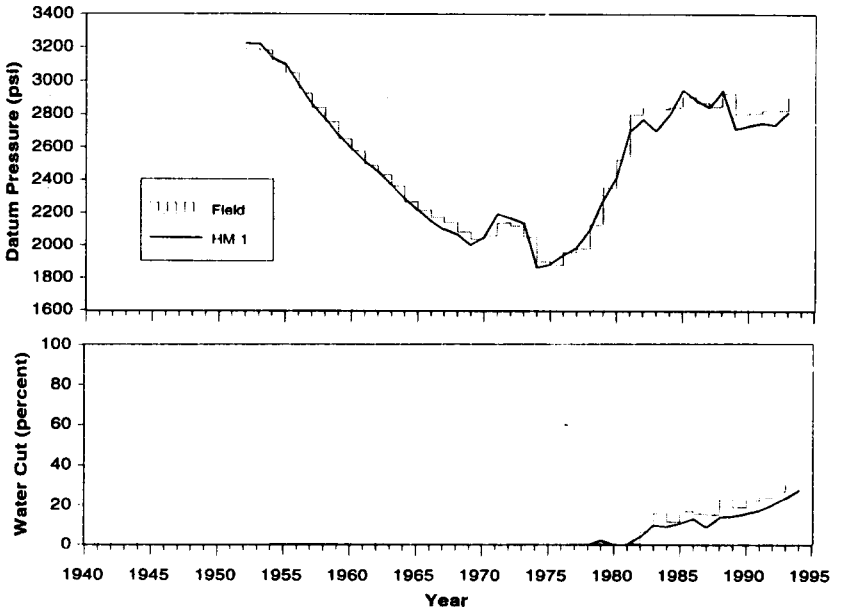

Figure 16: Comparison of model and field pressure and watercut (HM1)

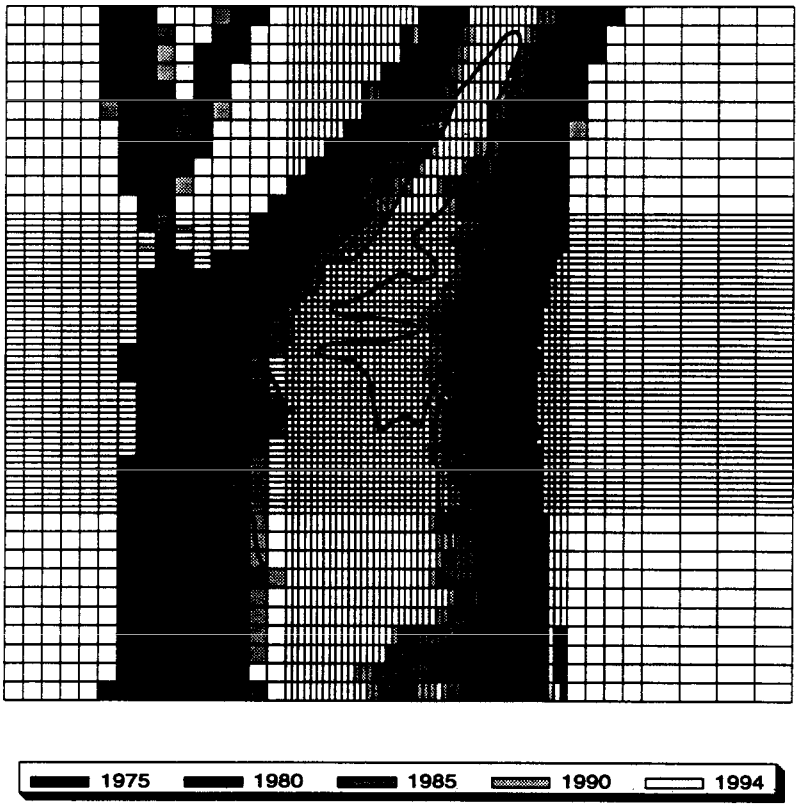

Figure 17: Flood front comparison (HM1)

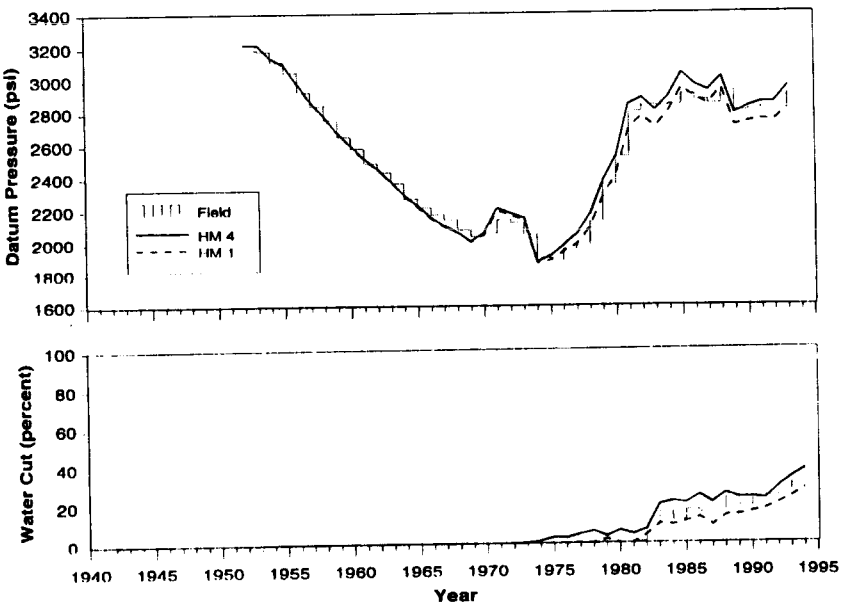

Figure 18: Comparison of model and field pressure and watercut (HM1 vs. HM4)

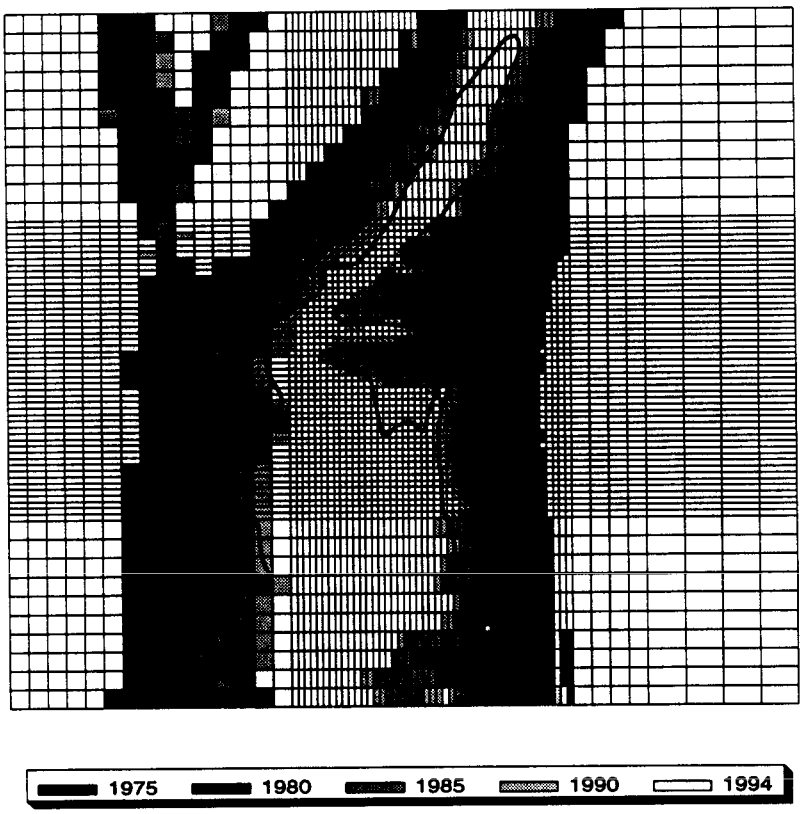

Figure 19: Flood front comparison (HM4)